Universiteit Leiden
The Netherlands

Understanding the surface structure of catalysts and 2D materials at the atomic scale
Boden, D.

Citation
Boden, D. (2023, September 12). *Understanding the surface structure of catalysts and 2D materials at the atomic scale*.

Theoretical Methods

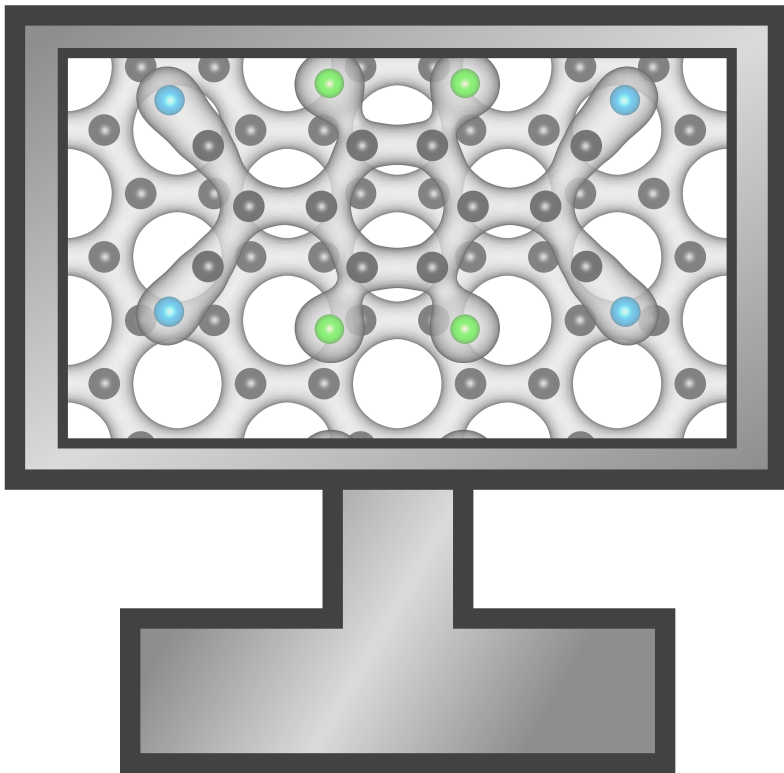In this chapter, theoretical tools are discussed, which are important for Chapters 4, 5, and 6. The methods used to evaluate the electronic structure, which underlie the adsorption energetics and the accompanying charge transfer are discussed in Section 3.1. Assuming an appropriate electronic structure can be obtained, a commonly used theoretical framework to simulate STM images, that can be used to assess the correlation between the theoretical description and experiment directly, is described in Section 3.2. Finally, Section 3.3 describes a method to facilitate analysis of surface structures found in experiments in Chapters 5 and 6 by extending energetics obtained in the microcanonical ensemble at zero temperature and pressure towards finite temperature and pressure conditions.

3.1 Electronic Structure Calculations

3.1.1 Born-Oppenheimer Approximation

The Born-Oppenheimer (BO) approximation is one of the most fundamental approximations in computational chemistry.[1] According to the BO approximation, the electrons adjust instantaneously to the motion of the nuclei, which means the motion of the nuclei and electrons can be decoupled. This is justified by the vast difference in mass between the nuclei and the electrons, resulting in a large disparity in the time-scales of their respective motions. As a result, the electronic structure and, in particular, the electronic ground state can be obtained separately for each set of nuclear positions by solving (an in practice usually approximated version of) the electronic Schrödinger equation.

3.1.2 Density-Functional Theory

Presently, the most common method used to calculate the electronic structure is density-functional theory (DFT), whereby the energy of an electronic system can be described by a functional of the electron density. The Hohenberg-Kohn theorem proves that the electronic ground-state energy and all other ground-state electronic properties can be uniquely determined by the electron density.[2] W. Kohn and L.J. Sham used a fictitious system of non-interacting electrons to determine the ground-state electron density, by solving a set of single-electron Kohn-Sham equations, which result from Hohenberg and Kohn's equivalent of the variational principle:

$$\left[-\frac{1}{2}\nabla^2 + v_{\text{e-e}}(\vec{r}) + v_{\text{e-N}}(\vec{r}) + v_{xc}(\vec{r}) \right] \psi_i(\vec{r}) = \epsilon_i \psi_i(\vec{r}) \quad . \tag{3.1}$$

Hartree atomic units are used here and in the remainder of this section. The first term is the kinetic energy operator, and ϵ_i is the energy of the Kohn-Sham orbital ψ_i. The single-electron potentials are divided into three separate potentials, describing the electron-electron interaction

$$v_{\text{e-e}}(\vec{r}) = \int \frac{\rho(\vec{r'})}{|\vec{r} - \vec{r'}|} d\vec{r'} \quad , \tag{3.2}$$

and the electron-nuclear interactions

$$v_{\text{e-N}}(\vec{r}) = \sum_I \frac{Z_I}{|\vec{r} - R_I|} \quad , \tag{3.3}$$

where Z_I and R_I are the charge and position of nucleus I, respectively. The positions of the nuclei (R_I) are kept constant while solving the Kohn-Sham equations, according to the aforementioned Born-Oppenheimer approximation. The electron density ($\rho(\vec{r})$ in Equations (3.2) and (3.3)) is obtained from the sum of the Kohn-Sham orbitals

$$\rho(\vec{r}) = \sum_i |\psi_i(\vec{r})|^2 \quad , \tag{3.4}$$

and the exchange-correlation potential is the functional derivative of the exchange-correlation energy E_{xc}:

$$v_{xc}(\vec{r}) = \frac{\delta E_{xc}[\rho]}{\delta\rho}(\vec{r}) \quad , \tag{3.5}$$

Since $v_{\text{e-e}}$ and v_{xc} in Equation 3.1 depend on the electron density explicitly, the Kohn-Sham equations have to be solved iteratively, until self-consistency has been reached within some numerical tolerance. In practice, the Kohn-Sham orbitals are expanded as linear combinations of basis functions taken from a particular set. In this work, plane waves are chosen as the most convenient basis functions.

Systematic errors in DFT stem from the approximation of the exchange-correlation functional $E_{xc}[\rho]$, since no exact expression is known. As such, a key focus of theoretical chemistry involves the development of exchange-correlation functionals that allow DFT to accurately reproduce, and predict, experimentally observed properties of materials. This means that the choice of an appropriate functional is important to obtain meaningful results with DFT.[3,4]

3.1.3 Analyzing Charge Transfer

A common "textbook" approach to describe chemical compounds is by considering them as a collection of atoms, held together by chemical bonds. This approach is easy to understand, and can be used to explain or predict many chemical properties of compounds. A quantum mechanical version of this approach, commonly called quantum theory of atoms in molecules (QTAIM), has been developed (primarily) by Richard Bader.

Bader shows that the volume associated with single molecules, or the unit cell of a crystal, can be divided into "Bader volumes" by determining dividing surfaces between their constituent atoms, at which the "flux of electrons" is zero.[5] In practice, this surface is a minimum in the electron density along the bonds between atoms or ions. Typically, each of the Bader volumes contains at most a single nucleus, and can therefore be considered as the atomic volume. By integrating separately over each of the Bader volumes, the Bader charge of each atom can be calculated from the number of electrons contained in that volume. Comparing the calculated Bader charges with the expected charge, given by the number of valence electrons of each atom, quantifies the charge transfer between the constituent atoms of the chemical compound, and thus

gives some insight into the type of bonding. An example of a Bader charge analysis for a diatomic molecule is shown in Figure 3.1.

The Henkelman group at the University of Texas has implemented this approach into a very versatile Fortran code, which is interfaced to electron densities that can be obtained from various DFT codes.[6–9] This code is used for all Bader charge analyses presented in this thesis.
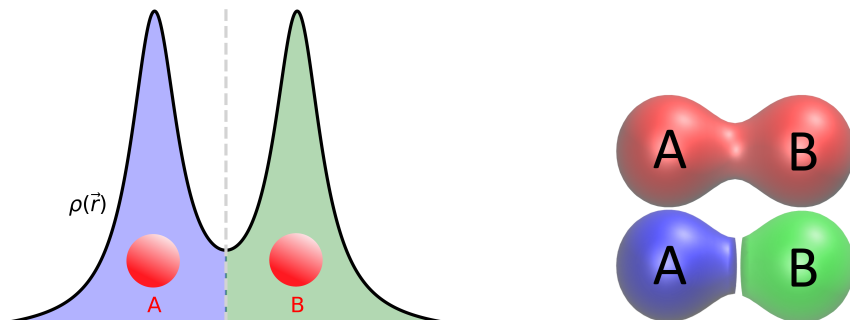
(a) One-dimensional cut through the electronic charge density $\rho(\vec{r})$ of an O_2 molecule. The nuclei of atom A and B are indicated by red circles, while $\rho(\vec{r})$ is shown on the y-axis. The surface of zero flux marked by the gray dashed line.

(b) Isosurface representation of the electronic charge density of an O_2 molecule (**top**) and corresponding charge densities assigned to nuclei A and B, according to the partitioning based on Bader volumes (**bottom**).

Figure 3.1: Schematic representation of a Bader charge analysis for an O_2 molecule. The electron density can be split up in two Bader volumes through a "surface of zero flux". The total Bader charge for atom A and B can be found by integrating $\rho(\vec{r})$ over the Bader volume that contains the nucleus of A (blue) and B (green), respectively.

3.2 Simulating STM Images

3.2.1 Bardeen's Formalism

In order to compare images from scanning tunneling microscopy (STM) experiments with first-principle calculations, an appropriate quantum mechanical description of the tunneling current is required. Here, we will discuss a formalism for the tunneling current, developed by John Bardeen.[10] By considering a time-dependent perturbation of the sample due to the tip, Bardeen's formalism is able to express the tunneling current as a function of the tip and sample states, temperature, and bias voltage. In the next section, the derivation of this expression for the tunnel current is given.[11,12]

The time-dependent Schrödinger equation describing the combination of the sample (S) and tip (T) can be defined as:

$$i\hbar \frac{\partial \Psi}{\partial t} = \left(-\frac{\hbar^2}{2m}\nabla^2 + U^S + U^T \right) \Psi \quad . \tag{3.6}$$

Where m describes the electron mass. When the sample and tip are far apart, so that they do not interact with one another, they can be described as two separate subsystems by the following set of two uncoupled Schrödinger equations:

$$i\hbar\frac{\partial\psi}{\partial t} = \hat{H}^{\square}\psi = \left(-\frac{\hbar^2}{2m}\nabla^2 + U^{\square}\right)\psi \text{ , with } \square = S, T \quad. \tag{3.7}$$

The Hamiltonian $\hat{H}^S$ contains the sample potential U^S and the Hamiltonian $\hat{H}^T$ contains the tip potential U^T. Stationary solutions of the uncoupled Schrödinger equations for the sample and tip take the form $\psi_\mu^S(\vec{r})e^{-iE_\mu^S t/\hbar}$ and $\psi_\nu^T(\vec{r})e^{-iE_\nu^T t/\hbar}$, respectively.

We now consider the tip moving slowly towards the surface, and thus let U^T in Equation 3.6 be a time dependent potential

$$U^T(t) = U^T e^{\eta t/\hbar} \tag{3.8}$$

where U^T is time-independent and equal to U^T in Equation 3.7, and $\frac{\eta}{\hbar}$ is very small and positive. In this way, the tip potential $U^T(t)$ is slowly turned on over time, as the tip approaches the sample. This means $U^T(t) \to 0$ for $t \to -\infty$, which results in Equation 3.7 for the sample. The rate at which $U^T(t)$ changes over time is determined by the value of $\frac{\eta}{\hbar}$, and $U^T(t) \to U^T$ for small $\frac{\eta}{\hbar}$ ($\frac{\eta}{\hbar} \to 0$), i.e., $U^T(t)$ becomes a time-independent potential in the limit of small sample-tip coupling.

Initially (for $t \to -\infty$), we can describe Ψ in Equation 3.6 as a linear combination of tip (ψ_ν^T) and sample (ψ_μ^S) eigenfunctions from the separated subsystems, i.e., the solutions from Equation 3.7, because tip and sample initially do not interact and thus U^S and U^T do not spatially overlap. Since the respective subsystems ψ_μ^S and ψ_ν^T are eigenfunctions of the Hamiltonians in Equation 3.7, they comprise an orthogonal and complete basis set for the Hamiltonian of the combined system given by Equation 3.6. Thus, the state $\psi(t)$, of the combined system, can be expanded in these solutions at all times

$$\psi(t) = a_\mu(t)\psi_\mu^S e^{-iE_\mu^S t/\hbar} + \sum_{\lambda=1}^{\infty} c_\lambda(t)\psi_\lambda^T e^{-iE_\lambda^T t/\hbar} \tag{3.9}$$

whereby state $\psi(t)$ is initially (at $t \to -\infty$) an eigenstate of the sample, since $a_\mu(-\infty) \to 1$ and $c_\nu(-\infty) \to 0$. The time-dependent coefficients for $t > -\infty$ have to be determined from Equation 3.6. Inserting Equations (3.7) and (3.9) into Equation 3.6 gives:

$$i\hbar\frac{\partial}{\partial t}(\psi(t)) = \left(\hat{H}^S + U^T(t)\right)\left(a_\mu(t)\psi_\mu^S e^{-iE_\mu^S t/\hbar}\right) + \left(\hat{H}^T + U^S\right)\left(\sum_{\lambda=1}^{\infty} c_\lambda(t)\psi_\lambda^T e^{-iE_\lambda^T t/\hbar}\right)$$

$$= a_\mu(t)\left[E_\mu^S + U^T(t)\right]\psi_\mu^S e^{-iE_\mu^S t/\hbar} + \sum_{\lambda=1}^{\infty} c_\lambda(t)\left(E_\lambda^T + U^S\right)\psi_\lambda^T e^{-iE_\lambda^T t/\hbar} \tag{3.10}$$

If we assume that the tip and sample eigenfunctions do not overlap ($\int \psi_\mu^S \psi_\nu^{T*} d\vec{r} \approx 0$),

and are orthogonal, we can project ψ_ν^T onto Equation 3.10[†] to obtain:

$$i\hbar\frac{\partial c_\nu(t)}{\partial t} = a_\mu(t)\left[E_\mu^S \cdot 0 + \int \psi_\mu^S U^T(t)\psi_\nu^{T*}d\vec{r}\right]e^{-i(E_\mu^S - E_\nu^T)t/\hbar} + $$
$$c_\nu(t)E_\nu^T + \sum_{\lambda=1}^{\infty} c_\lambda(t)\int \psi_\lambda^T U^S \psi_\nu^{T*}d\vec{r}\, e^{-i(E_\lambda^T - E_\nu^T)t/\hbar} \tag{3.11}$$

In what follows we only consider the time evolution during very short times, during which the time-dependent perturbation $U^T(t)$ is (almost) constant, so that we can assume $a_\mu \approx 1$ and $c_\nu \approx 0$. This simplifies Equation 3.11 to:

$$i\hbar\frac{\partial c_\nu(t)}{\partial t} = \int \psi_\mu^S U^T \psi_\nu^{T*}d\vec{r}\, e^{i(E_\nu^T - E_\mu^S - i\eta)t/\hbar} \tag{3.12}$$

By integrating Equation 3.12, we are able to obtain an expression for $c_\nu(t)$:

$$c_\nu(t) = \frac{-1}{\left(E_\nu^T - E_\mu^S - i\eta\right)}M_{\mu\nu}e^{i(E_\nu^T - E_\mu^S - i\eta)t/\hbar} \ , \ \ M_{\mu\nu} = \int \psi_\mu^S U^T \psi_\nu^{T*}d\vec{r} \tag{3.13}$$

Here, the tunneling matrix element $M_{\mu\nu}$ is introduced, which describes the transition from state μ in the sample to tip state ν due to the perturbed potential U^T. It is important to note that the tunneling matrix element $M_{\mu\nu}$ is only non-zero in the vacuum region between the tip and the sample, since $\psi_\nu^T \to 0$ in the region belonging to the sample, while $\psi_\mu^{S*} \to 0$ in the region belonging to the tip.

In order to get an expression for the tunnel current, the chance that an electron tunnels from the sample to the tip per unit time is required. The tunnel current for the transition between μ and ν, $P_{\mu\nu}$ can be obtained from Equation 3.13, since $P_{\mu\nu}(t) = \frac{\partial|c_\nu(t)|}{\partial t}^2$. This gives:

$$P_{\mu\nu}(t) = \frac{\partial|c_\nu(t)|^2}{\partial t} = \frac{2}{\hbar}\frac{\eta}{(E_\nu^T - E_\mu^S)^2 + \eta^2}|M_{\mu\nu}|^2 e^{2\eta t/\hbar} \tag{3.14}$$

In the limit of small tip-sample coupling, the last factor in Equation 3.14 simplifies according to: $\lim_{\eta \to 0} e^{2\eta t/\hbar} = 1$. Additionally, the second term is a type of Cauchy-Lorentz probability density function,[13] which means that $\lim_{\eta \to 0}\eta([E_\nu^T - E_\mu^S]^2 + \eta^2)^{-1} = \pi\delta(E_\nu^T - E_\mu^S)$. Equation 3.14 becomes:

$$P_{\mu\nu}(t) = \frac{2\pi}{\hbar}\delta(E_\nu^T - E_\mu^S)|M_{\mu\nu}|^2 \tag{3.15}$$

The tunnel current between states μ and ν can now be obtained by multiplying $P_{\mu\nu}$ by the charge per electron e. Since we are interested in the total tunneling current between the tip and the sample, and not the tunneling between 2 particular states, we have to sum over all tip states (ν) and sample states (μ). At finite temperatures, some states below the Fermi level are unoccupied and some states above the Fermi

---

[†]By applying $\int \psi_\nu^{T*}e^{iE_\nu^T t/\hbar}d\vec{r}\cdot$ on both sides of Equation 3.10.

level can be occupied. At thermodynamic equilibrium, the probabilities for populating those states are described by the Fermi-Dirac distribution function, which means the probabilities are

$$f(E - E_F) = \frac{1}{1 + e^{(E-E_F)/k_{\mathrm{B}}T}} \quad \text{for a state to be occupied and}$$

$$1 - f(E - E_F) \quad \text{for a state to be unoccupied,}$$

(3.16)

where T is the temperature and k_{B} is the Boltzmann constant. Since tunneling can only occur from filled states to empty states, Equation 3.15 has to be multiplied with the probability that μ is occupied and ν is unoccupied or vice-versa. At thermodynamic equilibrium, there is a certain tunnel current from states μ to states ν from the sample to the tip ($I_{S \to T}$) and vice-versa ($I_{T \to S}$). In an STM experiment, a bias voltage between the tip and the sample is applied to obtain a net tunneling current. For a bias voltage V applied to the sample, the resulting net tunneling current, I, can be calculated as follows:

$$I_{S \to T} = \frac{2e\pi}{\hbar} \sum_{\mu\nu} f(E_\mu^S - E_F^S + eV)[1 - f(E_\nu^T - E_F^T)]\delta(E_\nu^T - E_\mu^S)|M_{\mu\nu}|^2$$

$$I_{T \to S} = \frac{2e\pi}{\hbar} \sum_{\nu\mu} f(E_\nu^T - E_F^T)[1 - f(E_\mu^S + eV - E_F^S)]\delta(E_\mu^T - E_\nu^S)|M_{\mu\nu}|^2$$

$$I = I_{S \to T} - I_{T \to S} = \frac{2e\pi}{\hbar} \sum_{\mu\nu} \left[f(E_\mu^S - E_F^S + eV) - f(E_\nu^T - E_F^T) \right] \delta(E_\nu^T - E_\mu^S)|M_{\mu\nu}|^2$$

(3.17)

By changing the sign of the bias voltage, it is possible change the sign of I in order to tunnel through either the occupied or unoccupied states of the sample.

To further examine the tunneling matrix element $M_{\mu\nu}$, we define a plane Σ in the vacuum region between the tip and sample through which the tunneling occurs. This plane splits the vacuum region into a volume Ω^T, belonging to the tip, and a volume Ω^S, belonging to the sample. For the tip volume, Ω^T, by substituting for $U^T\psi_\nu^T = \left(\frac{\hbar^2}{2m}\nabla^2 + E_\nu^T \right)\psi_\nu^T$ from Equation 3.7 into the definition of the tunneling matrix element from Equation 3.13, we can rewrite $M_{\mu\nu}$ as:

$$M_{\mu\nu} = \int_{\Omega^T} \psi_\mu^S \left(E_\nu^T + \frac{\hbar^2}{2m}\nabla^2 \right) \psi_\nu^{T*} d\vec{r}$$

(3.18)

Assuming only elastic tunneling i.e., $E_\nu^T = E_\mu^S$, yields:

$$M_{\mu\nu} = \int_{\Omega^T} \psi_\mu^S E_\mu^S \psi_\nu^{T*} + \psi_\mu^S \frac{\hbar^2}{2m}\nabla^2 \psi_\nu^{T*} d\vec{r}$$

(3.19)

Substituting for E_μ^S using Equation 3.7:

$$M_{\mu\nu} = \int_{\Omega^T} \psi_\nu^{T*} \left(-\frac{\hbar^2}{2m}\nabla^2 + U^S \right) \psi_\mu^S + \psi_\mu^S \frac{\hbar^2}{2m}\nabla^2 \psi_\nu^{T*} d\vec{r}$$

$$= -\frac{\hbar^2}{2m} \int_{\Omega^T} \psi_\nu^{T*}\nabla^2\psi_\mu^S - \psi_\mu^S\nabla^2\psi_\nu^{T*} d\vec{r}$$
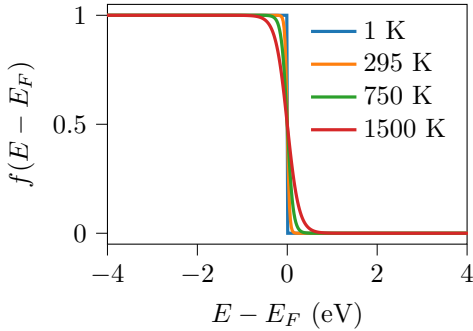
(3.20)

Figure 3.2: The Fermi-Dirac distribution from Equation 3.16 at various temperatures. At typical STM temperatures (295 K and below), $f(E - E_F)$ approaches a step-function.
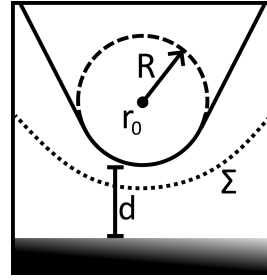

Figure 3.3: Schematic of the tip and surface in the Tersoff-Hamann approach.[14,15] The sample surface is indicated by the shaded area. At the point closest to the surface, the tip-sample distance is indicated by d, and the tip is presumed to locally have a spherical shape with radius R and center $\vec{r}_0$. A separation surface Σ in the vacuum region between the tip and surface is shown as a dotted line.

since in the region belonging to the tip, $U^S = 0$.

3.2.2 Tersoff-Hamann Approach

Using the formalism of Bardeen, we can estimate the tunneling current if we have information on the electronic wave functions of both the tip and the sample. In most STM experiments, the atomistic structure of the tip is not precisely known, which means that no accurate atomic-scale information about the tip states is available. On the other hand, for the analysis and interpretation of STM experiments, the exact (electronic) structure of the tip is only of interest to the degree in which it affects the STM imaging. The Tersoff-Hamann approach simplifies Equation 3.17 to enable practical computations of the tunneling current (and thus STM images) based on output that can nowadays be easily obtained from electronic structure calculations, typically done at the DFT level.[14,15]

Firstly, Equation 3.17 can be simplified by making some assumptions about the conditions of the (hypothetical) STM experiment. If we consider room temperature or below, which is often the case for STM experiments, the Fermi-Dirac distribution function approaches a step-function, as seen in Figure 3.2. Assuming that the Fermi level of the tip and sample is equivalent, in the limit of small bias voltage ($eV \ll E_\mu^S$), Equation 3.17 can be simplified to:

$$I = \frac{2\pi e^2 V}{\hbar} \sum_{\mu\nu} \delta(E_\mu^S - E_F)\delta(E_\nu^T - E_F)|M_{\mu\nu}|^2 \tag{3.21}$$

Now, to make solving Equation 3.21 easier, the tip is modeled as a spherically symmetric potential well with a local radius R, centered at a single point ($\vec{r}_0$) closest

to the surface, as shown in Figure 3.3. Since the potentials of the tip and sample are negligible at a surface Σ in the vacuum region, the states near the Fermi level of the tip and the sample satisfy the vacuum Schrödinger equation:

$$-\frac{\hbar^2}{2m}\nabla^2\psi(\vec{r}-\vec{r}_0) = -\phi\psi(\vec{r}-\vec{r}_0) \quad \text{or} \quad \left(\nabla^2 - \kappa^2\right)\psi(\vec{r}-\vec{r}_0) = 0 \qquad (3.22)$$

where ϕ is the work function, $\vec{r}$ a position in the vacuum region between the tip and the sample, and $\kappa = \sqrt{2m\phi}\hbar^{-1}$. Equation 3.22 is also known as the Helmholtz equation.[16]

Assuming the tip wave functions take the form of s-orbitals, Equation 3.22 has two types of solutions: spherical modified Bessel functions of the first and second kind. The spherical modified Bessel function of the first kind diverges far away from the tip ($\vec{r} \gg \vec{r}_0$), which means it does not satisfy the boundary condition for the tip wave functions ($\lim_{|\vec{r}-\vec{r}_0|\to\infty} \psi^T \to 0$).[17] The modified Bessel function of the second kind ($K_0(x)$) takes the form of an exponential decay from the center of the tip towards the vacuum and, therefore, satisfies the boundary condition for the tip wave functions.[18] This means the solutions of Equation 3.22 for the tip become:

$$\psi^T(\vec{r}-\vec{r}_0) = AK_0(\kappa|\vec{r}-\vec{r}_0|) = A\frac{e^{-\kappa|\vec{r}-\vec{r}_0|}}{\kappa|\vec{r}-\vec{r}_0|} \qquad (3.23)$$

where A is a normalization constant. Inserting ψ_ν^T from Equation 3.23 into Equation 3.20 gives:

$$M_{\mu\nu}(\vec{r}_0) = -\frac{\hbar^2}{2m}A\left[\int_{\Omega^T} K_0(\kappa|\vec{r}-\vec{r}_0|)\nabla^2\psi_\mu^S(\vec{r}-\vec{r}_0)d\vec{r} \right.$$
$$\left. -\int_{\Omega^T}\psi_\mu^S(\vec{r}-\vec{r}_0)\nabla^2 K_0(\kappa|\vec{r}-\vec{r}_0|)d\vec{r}\right] \qquad (3.24)$$

Because $U^S \to 0$ in Ω^T, the first integral can be treated as the vacuum Schrödinger equation in Equation 3.22, however, the second integral is not as straightforward to solve.

Using properties of the modified spherical Bessel functions, we can obtain a solution for Equation 3.24, in the form of:

$$M_{\mu\nu}(\vec{r}_0) = \frac{2\pi\hbar^2 A}{m\kappa}\psi_\mu^S(\vec{r}_0) \qquad (3.25)$$

Now that we have a convenient expression for $M_{\mu\nu}$, we can substitute it into Equation 3.21 to get

$$I = \frac{8\pi^3 A^2\hbar^3 e^2}{\kappa^2 m^2}V\rho^T(E_F)\sum_\nu |\psi_\nu^S(\vec{r}_0)|^2\delta(E_\nu^S - E_F) \qquad (3.26)$$

which gives

$$I = C \cdot V \cdot \rho^T(E_F) \cdot \rho^S(\vec{r}_0, E_F) \qquad (3.27)$$

with

$$C = \frac{8\pi^3 A^2 \hbar^3 e^2}{\kappa^2 m^2} \quad (3.28) \quad \text{and} \quad \rho(\vec{r}, E) \equiv \sum_\lambda |\psi_\lambda(\vec{r})|^2 \, \delta(E_\lambda - E) \quad (3.29)$$

This means that in the Tersoff-Hamann approximation the tunneling current can be calculated from a constant, C, the bias voltage, V, the density of states of the tip at the Fermi level, $\rho^T(E_F)$, and the local density of states (LDOS) of the sample at the center of curvature of the tip near the Fermi level, $\rho^S(\vec{r}_0, E_F)$. As expected, $I \propto e^{-2\kappa d}$, since from 3.23 and the definition of r_0 in Figure 3.3 we know that $|\psi_\nu^S(\vec{r}_0)|^2 \propto e^{-2\kappa(R+d)}$.

As mentioned in Section 2.4, STM experiments can either be performed in constant-height mode, where the tip-sample distance (d) is kept constant and the tunnel current (I) is measured, or in constant-current mode, where the tunnel current is kept constant and the tip-sample distance is measured. Due to the exponential decay of I with increasing d, the Tersoff-Hamann approach enables meaningful simulations of STM images even if C and $\rho^T(E_F)$ are not accurately known. In fact, the results in Equation 3.27 show that in the case of constant-current STM, the tip will simply follow a surface of constant local density of states of the sample, since the only positional dependence of $I(\vec{r}_0)$ is contained in $\rho^S(\vec{r}_0, E_F)$. This means it is possible to model a constant-current STM image from first-principles by calculating the LDOS of the sample at the surface, and plotting an isosurface of the LDOS at the energy that corresponds to the bias voltage applied in the experiments.

Since the tip states are approximated as s-orbitals (given by K_0 in Equation 3.23), the Tersoff-Hamann approach holds only if the electronic states of the real tip have a low angular dependence. When the effective tip radius (R) becomes larger, the contribution of real wave functions with higher angular momentum l becomes more significant, and the approach becomes less realistic. In order to overcome this problem with the Tersoff-Hamann approach, Chen[17] developed an extension of the Tersoff-Hamman approach, wherein the tip wave function in the vacuum region is expanded in terms of spherical harmonics. This results in solutions of the tunneling matrix elements for higher order orbitals that are related also to the derivatives of the sample wave functions at the tip position ($\vec{r}_0$), and allow for a more exact description of the tunneling process. The results obtained with the standard Tersoff-Hamann approach suggest that it is sufficient in the scope of this work.

3.3   Atomistic Thermodynamics

At high gas pressures and non-zero temperatures, the surface of a heterogeneous catalyst is exposed to a high impingement rate of molecules from the gas phase, which are continuously adsorbing and desorbing. The relative stability of different candidate surface structures at these conditions cannot be determined by directly comparing the relative total energy from total energy calculations if such structures contain different adsorbate coverages and/or surface atom densities.[19] Increasing the amount of (adsorbate) molecules will, without any additional considerations, change the calculated absolute total energy of the system, because atoms are 'created' from nothing. A direct comparison between structures with different atomic compositions is thus meaningless

if the origins of the atoms that are added, or removed, are not accounted for. As such, to represent a surface at thermodynamic equilibrium, a grand-canonical description of the atoms and molecules on the surface is required. The foundation of atomistic thermodynamics is to accommodate this by including gas-phase and solid-state reservoirs. These reservoirs can provide or take away constituents from a particular surface structure, which enables the construction of thermodynamic phase diagrams based on the results of total energy calculations of surfaces with different numbers of adsorbates and/or surface atoms.[20,21]

If the surface is at equilibrium with the gas phase, then the structure that is the most thermodynamically stable at constant temperature T and partial pressures p_g (for each gas g) is the structure with the minimal surface Gibbs free energy

$$\gamma(T, p_g) = \frac{1}{A}[G(T, p_g, N_g, N_s) - \sum_g N_g \mu_g - \sum_s N_s \mu_s] \tag{3.30}$$

In equation 3.30, $G(T, p_g)$ is the Gibbs free energy of the surface configuration, N_g and N_s are the number of species with a reservoir in the gas phase, with chemical potential μ_g, and surface-only species with chemical potential μ_s, respectively. To evaluate equation 3.30, suitable reservoirs have to be determined for all species involved to determine their chemical potential.[22] For species g, the gas phase is an obvious choice. By approximating the gas as an ideal gas, μ_g in equation 3.30 can simply be looked up in a database.[23] Often, equation 3.30 is easier to evaluate by introducing a reference surface structure with N_g^* gas-phase species, N_S^* surface species, and a surface free energy of $\gamma_0(T, p_g)$, which yields

$$\gamma(T, p_g) - \gamma_0(T, p_g) = \frac{1}{A} \sum_{g,s} \left[\Delta G(T, p_g, N_g, N_s, N_g^*, N_s^*) - \Delta N_g \mu_g - \Delta N_s \mu_s \right] \tag{3.31}$$

with

$$\Delta N_g = N_g - N_g^* , \quad \Delta N_s = N_s - N_s^*$$

and

$$\Delta G(T, p_g, N_g, N_s, N_g^*, N_s^*) = G(T, p_g, N_g, N_s) - G_0(T, p_g, N_g^*, N_s^*). \tag{3.32}$$

In the case of atomistic thermodynamics calculations whereby the number of surface species N_s in equation 3.31 does not change, for example when comparing only the stability of various adsorption structures, $\Delta N_s = 0$ and therefore μ_s does not have to be considered. When $\Delta N_s \neq 0$, for example when a (component of) a catalyst is reduced or oxidized, the bulk phase is a suitable reservoir. This leaves ΔG as the only part of equation 3.31 that still has to be determined. The absolute Gibbs free energy is consists in its general form of the following terms

$$G = E^{tot} + F^{trans} + F^{rot} + F^{vib} + F^{conf} + pV, \tag{3.33}$$

and is usually difficult to calculate exactly. However, F^{trans} and F^{rot} can be discarded for solids and pV constitutes only a small fraction of G.[24] The terms that contribute

most significantly to the total Gibbs free energy in a solid are E^{tot}, which is the total energy, and the vibrational free energy F^{vib}.[24,25] If a proper reference surface structure is chosen in equation 3.31 and all considered surface structures do not vary a great deal, then the ΔF^{vib} and ΔF^{conf} will be relatively small and can be neglected in a first approximation.[25] For $\Delta\mu_g \equiv \mu_g - E^{tot}(g)$, where $E^{tot}(g)$ is the total energy of the isolated gas species g and $E^{tot}(s)$ the total energy of the solid-state reservoir of species s, then equation 3.31 can be simplified to

$$\gamma(T, p_g) - \gamma_0(T, p_g) \approx \frac{1}{A}[\Delta E^{tot} - \Delta N_g \Delta\mu_g(T, p_g)], \qquad (3.34)$$

where

$$\Delta E^{tot} = E^{tot}(N_g, N_s) - E^{tot}(N_g^*, N_s^*) - \Delta N_g E^{tot}(g) - \Delta N_s E^{tot}(s) \qquad (3.35)$$

According to the approximation given by Equation 3.34, the excess surface free energy of a given structure can be obtained from total energy calculations of the corresponding structure, of the reference surface, of all isolated gas-phase species and of the associated solid-state reservoirs. Pressure and temperature dependence is included in $\Delta N_g \Delta\mu_g(T, p_g)$, whereby $\Delta\mu_g(T, p_g)$ can be determined from reference tables. This means that –within these approximations– atomistic thermodynamics is computationally very convenient. Nevertheless, it is important to note that the change in vibrational free energy, ΔF^{vib}, and the change in configurational free energy, ΔF^{conf}, are not always negligible. In that case, ΔF^{vib} can either be approximated,[26] or calculated in more detail from first principles.[27,28] ΔF^{conf} is not so straightforward, but can often be quantified using cluster expansion techniques that can help with the calculation of total energies for a huge amount of surface structures.[29,30] This holds in particular for ordered surface structures, which do not contain any "complex" reconstructions or overstructures.

To apply atomistic thermodynamics for the prediction of surface structures present *in situ* on catalysts, multiple gas phase reactants and products usually have to be accounted for. This means that in equation 3.34 each molecule type has its respective reservoir. As mentioned before, the surface equilibrium structure is determined as a function of partial pressures and temperature, but for a full thermodynamic equilibrium the gas phase reservoirs are in equilibrium also. Under catalytic conditions the gas phase is obviously not in equilibrium, otherwise all reactants would be converted to the more thermodynamically favorable products. Obviously, this is not a proper description of the conditions during catalysis, so to prevent this from happening, the gas phase reservoirs cannot be in equilibrium with each other. "Constrained" atomistic thermodynamics describe a situation where the surface is in equilibrium with the gas phase consisting of reactant reservoirs that are independent of one another. This approximation allows for first-principle comparison of surface structures under different reaction conditions.

By applying the constrained equilibrium approximation to equation 3.34, it is possible to evaluate the surface free energies of a range of candidate structures as a function of each gas-phase chemical potential $\Delta\mu_g(T, p_g)$. The temperature and pressure dependence of the surface free energy in equation 3.34 is contained in the gas-phase chemical

potentials, so the most stable surface structure can also be determined as a function of pressure at a constant temperature or as a function of temperature at constant pressure. Consequently, a phase diagram, as a function of temperature and partial pressure, can be obtained by determining the structure with the minimum surface free energy for every combination of gas phase chemical potentials.

It is important to emphasize that (constrained) atomistic thermodynamics does not take into account the influence of kinetic effects, such as reactions between species on the surface. If catalytic activity consumes surface(-bound) species faster than they can be replenished from the gas phase, or if various species are consumed at a drastically different rate, the predicted structure from constrained atomistic thermodynamics may differ from the one formed in experiments, let alone real (commercial) catalysts. To ensure meaningful results, it is important that the inherent approximations of atomistic thermodynamics are appropriate to model the experimental conditions. Another limitation that currently holds true for all atomistic thermodynamics approaches is that the reliability of the results depend on the chemical intuition and creativity of the theoretician, as it is only possible to compare between (surface) structures that are included explicitly. In other words, structures that are not explicitly considered in the calculations cannot be obtained as a result, even if those structures are thermodynamically more favorable.

3

References

(1) Born, M.; Oppenheimer, R. *Annalen der Physik* **1927**, *389*, 457–484.

(2) Hohenberg, P.; Kohn, W. *Physical Review* **1964**, *136*, B864–B871.

(3) Medvedev, M. G.; Bushmarinov, I. S.; Sun, J.; Perdew, J. P.; Lyssenko, K. A. *Science* **2017**, *355*, 49–52.

(4) Lejaeghere, K. et al. *Science* **2016**, *351*, aad3000.

(5) Bader, R. F. W. *The Journal of Physical Chemistry A* **2007**, *111*, 7966–7972.

(6) Yu, M.; Trinkle, D. R. *The Journal of Chemical Physics* **2011**, *134*, 064111.

(7) Tang, W.; Sanville, E.; Henkelman, G. *Journal of Physics: Condensed Matter* **2009**, *21*, 084204.

(8) Sanville, E.; Kenny, S. D.; Smith, R.; Henkelman, G. *Journal of Computational Chemistry* **2007**, *28*, 899–908.

(9) Henkelman, G.; Arnaldsson, A.; Jónsson, H. *Computational Material Science* **2006**, *36*, 354–360.

(10) Bardeen, J. *Physical Review Letters* **1961**, *6*, 57–59.

(11) Lounis, S., *Theory of Scanning Tunneling Microscopy*; Cornell University Library: 2014, p 7827531188.

(12) Gottlieb, A. D.; Wesoloski, L. *Nanotechnology* **2006**, *17*, R57–R65.

(13) Lee, H.-Y.; Park, H.-J.; Kim, H.-M. *Communications for Statistical Applications and Methods* **2014**, *21*, 183–191.

(14) Tersoff, J.; Hamann, D. R. *Physical Review Letters* **1983**, *50*, 1998–2001.

(15) Tersoff, J.; Hamann, D. R. *Physical Review B* **1985**, *31*, 805–813.

(16) White, H.; Bailey, P.; Lawrence, J.; George, J.; Vera, J. *Physics Open* **2019**, *1*, 100009.

(17) Chen, C. J. *Physical Review B* **1990**, *42*, 8841–8857.

(18) Abramowitz, M.; Stegun, I. A., *Handbook of Mathematical Functions with Formulas, Graphs, and Mathematical Tables*; United States Department of Commerce: Washington, D.C., 1972.

(19) Gross, A., *Theoretical Surface Science: A Microscopic Perspective*; Springer: 2009.

(20) Sutton, C.; Levchenko, S. V. *Frontiers in Chemistry* **2020**, *8*, 757.

(21) Rogal, J.; Reuter, K. *Ab initio atomistic thermodynamics for surfaces: A primer*; tech. rep.; Berlin: Fritz-Haber-Institut der Max-Planck-Gesellschaft, 2006.

(22) Reuter, K. *Catalysis Letters* **2016**, *146*, 541–563.

(23) Stull, D. R.; Prophet, H.; States., U., *JANAF thermochemical tables*, 2d ed.; U.S. Dept. of Commerce, National Bureau of Standards: 1971.

(24) Reuter, K.; Scheffler, M. *Physical Review B* **2001**, *65*, 035406.

(25) Rogal, J.; Reuter, K.; Scheffler, M. *Physical Review B* **2004**, *69*, 075421.

(26) Sun, Q.; Reuter, K.; Scheffler, M. *Physical Review B* **2004**, *70*, 235402.

(27) Pavone, P.; Karch, K.; Schütt, O.; Strauch, D.; Windl, W.; Giannozzi, P.; Baroni, S. *Physical Review B* **1993**, *48*, 3156–3163.

(28) Ghosez, P.; Cockayne, E.; Waghmare, U. V.; Rabe, K. M. *Physical Review B* **1999**, *60*, 836–843.

(29) Sanchez, J. M. *Physical Review B* **1993**, *48*, 14013–14015.

(30) Gonis, A.; Zhang, X.; Freeman, A. J.; Turchi, P.; Stocks, G. M.; Nicholson, D. M. *Physical Review B* **1987**, *36*, 4630–4646.

3